catalysts

MDPI

Article

Composition, Structural Evolution and the Related Property Variations in Preparation of Mixed Cesium/Ammonium Acidic Salts of Heteropolyacids

Heng Zhang *, Tingting Wang, Xinxin Ma and Wancheng Zhu

School of Chemistry and Chemical Engineering, Qufu Normal University, Qufu 273165, China; ttlme@126.com (T.W.); qsdhgyl@163.com (X.M.), zhuwancheng@tsinghua.org.cn (W.Z.)

* Correspondence: zhangheng@mail.qfnu.edu.cn; Tel.: +86-537-4453130

Academic Editor: Ivan V. Kozhevnikov

Received: 26 October 2016; Accepted: 23 November 2016; Published: 29 November 2016

Abstract: The composition, structural evolution and the related property variations of mixed cesium/ammonium acidic salts of heteropolyacids were investigated in detail by tracking and analyzing the initial precipitates, evaporation residues and the calcined products in their preparation process. Results show that V cannot completely enter the heteropolyanions in the initial precipitates when the Cs^+ added amount is low, and the increase in Cs^+ adding amount improves the substitution of V for Mo in the heteropolyanions. Both the initial precipitates and the evaporation residues are mixtures of cesium and ammonium salts of heteropolyacids before calcination. Thermal treatment causes the decomposition of the ammonium salts and the formation of single-phase solid solutions from mechanical mixtures. The calcined products of the initial precipitates and the evaporation residues vary greatly in textural properties. The determinants of the catalytic performance for the oxidation of methacrolein to methacrylic acid are acidity and specific surface area of the compounds. The increase in specific surface area mainly improves the conversion of methacrolein, but not the selectivity of methacrylic acid. Insufficient acidity caused by high Cs^+ content in the compounds is responsible for the low selectivity.

Keywords: heteropoly compound; structural evolution; catalytic property; selective oxidation

1. Introduction

Heteropoly compounds (HPCs) have attracted great attention as effective catalysts for redox and acid-catalyzed reactions, especially in the production processes of petroleum and coal downstream products, such as the oxidative dehydrogenation of alkanes [1,2], the oxidation of propylene/propane to acrolein/acrylic acid [3,4], the oxidation of *iso*-butane/methacrolein (MAL) to methacrylic acid (MAA) [5,6], and an increasing number of newly emerging fields [7–10].

It is well known that the structure of Keggin-type HPCs can be subdivided into the primary, secondary and tertiary structure [11]. In the primary structure, i.e., the heteropolyanion, such as $[PMo_{12}O_{40}]^{3-}$, the central phosphorus atom is located at the center of a PO_4 tetrahedron, which is surrounded by twelve MoO_6 octahedra. The three-dimensional arrangement of heteropolyanions and counterions, perhaps also including water of crystallization and some additional molecules, is called the secondary structure. There are important relationships between the catalytic function and the primary or the secondary structure of HPCs. It has been reported that V can partially substitute for Mo in the heteropolyanions and improve the catalytic property for selective oxidation reactions [12,13]. In particular, effective catalysts can be designed and prepared by controlling the distribution of vanadyl species in the primary or secondary structure [14]. Compared with the parent heteropolyacids, the formation of acidic salts with alkaline metals is effective on both the activity and stability of

the catalysts. It has also been reported that the addition of transition metals as counterions greatly affects the activity of a catalyst by improving the physico-chemical properties, especially the redox property [13,15]. For the vapor-phase selective oxidation of MAL to MAA, our previous works have found that Cu and Fe as counterions in HPCs significantly improve the redox property and thereby enhance the catalytic behavior [16,17]. In addition to the primary and secondary structure, the tertiary structure, which refers to particle size, pore structure, surface area, uniformity of composition and so on, also has great effect on the catalytic function. It has been found that the pores in HPCs are interparticle, not intracrystalline, according to N_2 adsorption measurement, and the surface areas of HPCs are significantly dependent on the size of the counterions. Lee et al. [18] reported that the surface areas of $Cs_xH_{4-x}PMo_{11}VO_{40}$ were 2.6, 11.2, 10.0, 130, 164, and 103 $m^2 \cdot g^{-1}$ for x = 0, 1, 2, 3, 3.5, and 4, respectively. In the case of $Cs_x(NH_4)_{3-x}HPMo_{11}VO_{40}$, the surface areas were 3.5, 5.8, 8.4, 16.4, 58.6, and 87.6 $m^2 \cdot g^{-1}$ for x = 0, 0.5, 1.5, 1.7, 2.5, and 3, respectively [19]. Significant difference can be found in surface area for the compound $Cs_3HPMo_{11}VO_{40}$ prepared by different methods.

Because the salts of heteropolyacids with large monovalent ions, such as Cs^+, NH_4^+, are insoluble in water or other polar solvents, precipitate is generated in the heteropolyacids solution after the addition of these ions, and then the obtained slurry is usually evaporated to dryness to get the acidic cesium or ammonium salts. It was found that the mechanism of pore formation for $(NH_4)_xCs_yH_{0.5}PW_{12}O_{40}$ exhibited a significant difference when it was synthesized through a precipitation/ion exchange process with a different addition order for each cation [20]. It was also found that the addition method of NH_4^+ in the precursors for preparing Cu- and Fe-doped acidic cesium salts of molybdovanadophosphoric acid greatly affected the phase composition and catalytic property of the calcined catalysts in our previous work [16]. These results show that the structure and property of the mixed cesium and ammonium salts of heteropolyacids are variable depending on the precipitation process. However, there was almost no previous work conducting detailed studies on the composition and structural evolution in the preparation steps, including precipitation, water removal and calcination. The differences in the composition, physico-chemical properties and catalytic ability of the calcined HPCs catalysts prepared using the initial precipitates and the evaporation residues as the precursors, respectively, have not been explored. Herein, the synthesis of cesium/ammonium mixed acidic salts of molybdovanadophosphoric acid with two different methods for the removal of water before calcination is reported. A detailed comparison between the initial precipitates and the evaporation residues was performed. The relative contents of Cs^+, NH_4^+ and H^+ in the catalysts prepared using two different precursors with different Cs^+ adding amount were determined, and the influence factors of the structure, redox property, textural properties as well as catalytic ability of the catalysts were evaluated and discussed.

2. Results and Discussion

2.1. Elemental Differences between the Initial Precipitates and the Evaporation Residues

The chemical composition analysis of HPCs has fundamental importance for the determination of the composition and structure of heteropolyanions and counterions, which directly affect the redox and acidic properties of the compounds. The plasma atomic emission spectroscopy (ICP-AES) results of the initial precipitates and the evaporation residues are given in Table 1. The element ratios of the samples obtained by evaporation are in agreement with the preparation stoichiometry, while the initial precipitates exhibit comparatively different elementary composition. In the initial step for the preparation of the compounds, H_3PO_4, MoO_3 and NH_4VO_3 were mixed and reacted for the formation of Keggin-type HPCs. It was supposed that the heteropolyanion was $[PMo_{11}VO_{40}]^{4-}$ and the counterions were H^+ and NH_4^+, that is the initial HPCs were probably a mixture of $H_4PMo_{11}VO_{40}$ and its ammonium salt. After $CsNO_3$ was added to the slurry, it reacted with $H_4PMo_{11}VO_{40}$, generating insoluble cesium salt. Thus, the initial precipitates should be a mixture of cesium and ammonium salts of heteropolyacids. Under the assumption that the precipitates were composed of $Cs_4PMo_{11}VO_{40}$

and $(NH_4)_4PMo_{11}VO_{40}$, the theoretical mole ratios of Cs/P for 1Cs-F, 2Cs-F, 3Cs-F were 2, 2.67 and 3, respectively, which were higher than the actual mole ratios according to the ICP-AES results, and the disparities of the actual and the theoretical value decreased with the increase of Cs^+ adding amount. Meanwhile, it can be found that the mole ratio of Mo/P decreased with the increase of Cs^+ adding amount and the mole ratio of V/P was in the opposite way as shown in Table 1. The above results indicate that V could not completely enter the heteropolyanions when the Cs^+ added amount was low, and the heteropolyanions probably included $[PMo_{12}O_{40}]^{3-}$ in addition to $[PMo_{11}VO_{40}]^{4-}$. Moreover, the increase of Cs^+ adding amount was helpful to promote the substitution of V for Mo in the heteropolyanions.

Table 1. Elemental analysis of the samples.

Sample	Atomic Ratio		
	Mo/P	V/P	Cs/P
1Cs-E	11.0	1.0	1.0
2Cs-E	10.9	1.1	1.9
3Cs-E	11.1	1.1	3.0
1Cs-F	11.5	0.7	1.7
2Cs-F	11.3	0.9	2.4
3Cs-F	10.9	1.0	2.9

2.2. Structure Analysis of the Initial Precipitates and the Evaporation Residues

It is well known that there are usually four strong characteristic bands between 1100 and 700 cm^{-1} in the Flourier transformation infrared (FT-IR) spectra of Keggin-type molybdophosphoric HPCs, which are related to the P–O_a, Mo–O_d, Mo–O_b–Mo and Mo–O_c–Mo asymmetric stretching vibrations, respectively [21,22]. The FT-IR spectra of the samples are shown in Figure 1a, which indicate that all the samples exhibit Keggin structure and the characteristic bands are observed at 1061 cm^{-1} (P–O_a), 966 cm^{-1} (Mo–O_d), 865 cm^{-1} (Mo–O_b–Mo), and 795 cm^{-1} (Mo–O_c–Mo). There is a band related to the N–O asymmetric stretching vibration of the NO_3^- anions at 1385 cm^{-1} in the spectra of 2Cs-E and 3Cs-E, while it does not appear in that of 1Cs-E. NO_3^- anions were coming from the raw material of $CsNO_3$ and they might combine with H^+ to form HNO_3 following the formation of the precipitate as cesium salt of heteropolyacids. The formed HNO_3 tends to decompose during evaporation and drying of the precursors, resulting in the disappearance of NO_3^- anions from the sample with a low adding amount of $CsNO_3$. There is a band related to the N–H deformation vibration of the NH_4^+ cations at 1413 cm^{-1} in the spectra of the samples and its intensity decreases with the increase of Cs^+ content. The reasons for that can be attributed to two aspects: firstly, the relative content of ammonium salts decreases with the increase of cesium salts of heteropolyacids in the samples, and, secondly, NH_4^+ in the ammonium salts of heteropolyacids might be substituted by Cs^+ when the content of Cs^+ is high. As shown in Figure 1a, a shoulder peak of the P–O_a band at 1076 cm^{-1} and a shoulder peak of the Mo–O_d band at 997 cm^{-1} are observed in the FT-IR spectra of the samples, which represent the incorporation of V into the Keggin structure of $H_3PMo_{12}O_{40}$ with decreased oxoanion symmetry as revealed in some previous works [22,23].

The X-ray diffraction (XRD) patterns of the samples are shown in Figure 1b, which showed that the main phase of all the samples possesses cubic secondary structure as Keggin-type HPCs. The characteristic diffraction peaks of $Cs_4PMo_{11}VO_{40}$ are illustrated in Figure 1b, besides which some characteristic diffraction peaks representing ammonium salts are also observed at 2θ = 15.2°, 21.6°, 36.1°, and 39.4° in the patterns of the samples before calcination. Thus, the obtained solids, no matter the initial precipitates or the evaporation residues, are mixtures of cesium and ammonium salts of heteropolyacids before calcination. According to the obvious change in the intensity of the diffraction peaks at 15.2° and 21.6°, it is confirmed that the content of ammonium salt in the obtained solid decreased with the increase of Cs^+ adding amount. The patterns of 1Cs-E consist of a split peak

(2θ = 8.9°–9.1°), which is considered to be associated with the heteropolyacid in a triclinic crystal form [24,25] and it does not appear in the patterns of the samples with higher content of Cs^+.

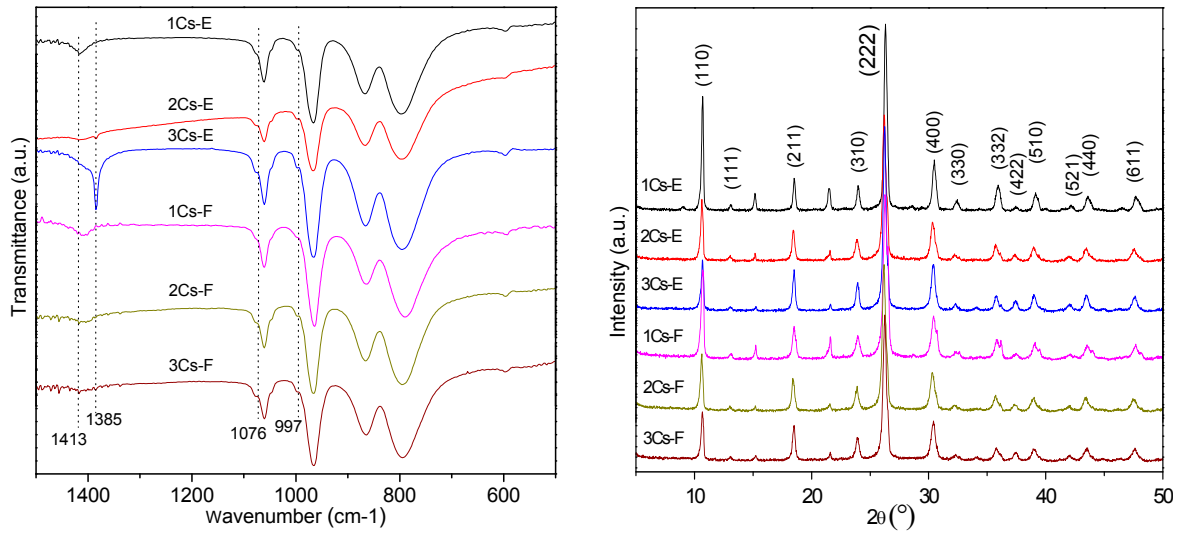

Figure 1. Flourier transformation infrared (FT-IR) spectra (**a**); and X-ray diffraction (XRD) patterns (**b**) of the initial precipitates and the evaporation residues.

^{31}P magic angle spinning nuclear magnetic resonance (MAS NMR) is a useful technique for providing structural information of phosphorous-containing HPCs by exploring the chemical environment of phosphorous. Figure 2 displays the ^{31}P MAS NMR spectra of the initial precipitates and the evaporation residues. There are two main ^{31}P resonance peaks in the spectra of all the samples. One of them is in the range of –3.60 to –3.54 ppm and the other is in the range of −4.44 to −4.35 ppm, representing two different phosphorous nucleus environments in the samples. The latter can be assigned to $Cs_4PMo_{11}VO_{40}$ as has been reported in the literature [26], and the former is assigned to hydrated acidic ammonium salts of $H_3PMo_{12}O_{40}$ or $H_4PMo_{11}VO_{40}$. This confirms that the initial precipitates and the evaporation residues are mixtures of cesium and ammonium salts of heteropolyacids, which is in agreement with the XRD measurement. In addition to those two main peaks, a small peak in the range of −2.72 to −2.60 ppm is observed in the spectra of 2Cs-F, 3Cs-F, 2Cs-E, and 3Cs-E, which can be assigned to dehydrated acidic ammonium salts [27,28]. Moreover, two peaks at 2.89 and 0.55, respectively, appeared in the spectra of 3Cs-E, representing the presence of at least two more different phosphorous containing species in this sample. The comparison of 3Cs-F and 3Cs-E in ^{31}P MAS NMR spectra indicates that the evaporation process in preparing the catalyst precursors affects their basic structure and composition.

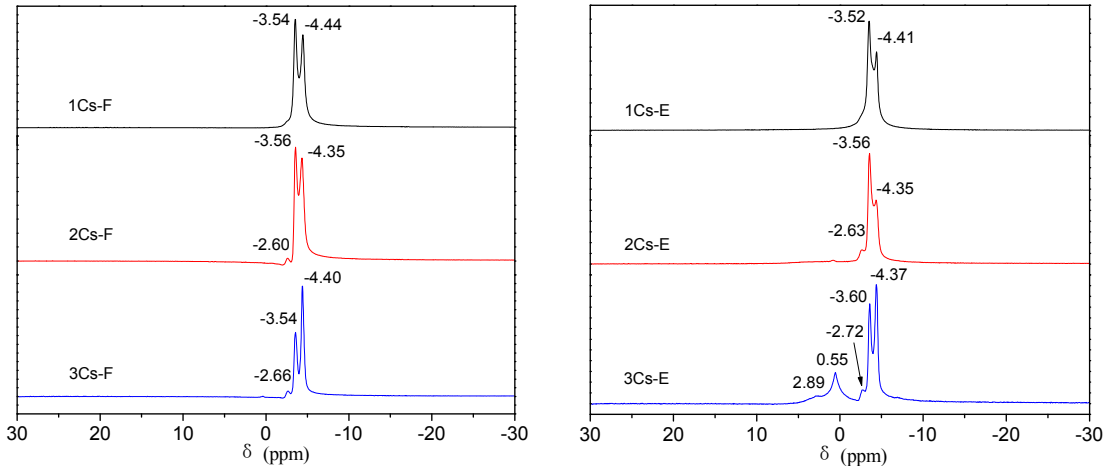

Figure 2. ^{31}P magic angle spinning nuclear magnetic resonance (MAS NMR) spectra of (**a**) the initial precipitates and (**b**) the evaporation residues.

2.3. Structural Evolution during the Calcination Process

The FT-IR spectra and XRD patterns of the initial precipitates and the evaporation residues after calcination are shown in Figure 3. As shown in Figure 3a, a band at 1034 cm^{-1} appears in the spectra of 1Cs-E, 1Cs-F, 2Cs-E and 2Cs-F after calcination, but is not found in the spectra of 3Cs-E and 3Cs-F. The appearance of this band is accompanied with the decrease of the shoulder peaks of the P-O_a and Mo–O_d. This band has been assigned to the VO^{2+} species generated from the migration of V from the Keggin units to the cationic position [29,30]. The above results show that the increase of Cs^+ as counterions promotes the stability of the $[PMo_{11}VO_{40}]^{4-}$ heteropolyanions. After calcination, the XRD patterns of the samples show the following changes: (1) the intensity of the diffraction peaks at 2θ = 15.2° and 21.6° decrease significantly; (2) the diffraction peaks at 2θ = 36.1° and 39.4° disappear; and (3) the split peak in the patterns of 1Cs-E disappears. The above results reveal that thermal treatment causes the decomposition of the ammonium salt in the samples and promotes the formation of single-phase solid solution from a mechanical mixture.

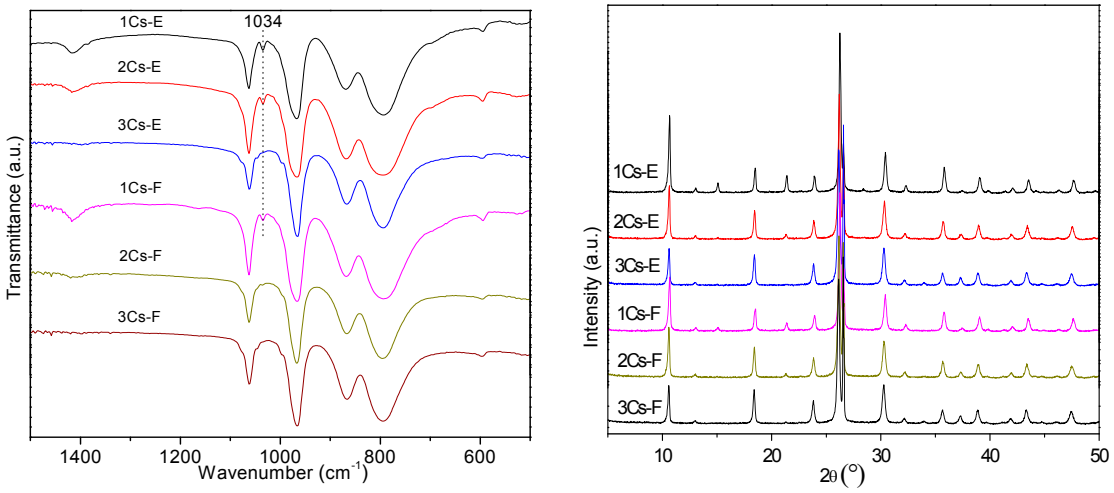

Figure 3. FT-IR spectra (**a**); and XRD patterns (**b**) of the initial precipitates and the evaporation residues after calcination.

2.4. Determination of the Relative Content of Counterions in Calcined Compounds

NH_3 temperature-programmed desorption (NH_3-TPD) was used to evaluate the acidity of the calcined compounds and the results are shown in Figure 4. Besides the general NH_3-TPD test, every sample was also tested by the same procedure only without ammonia adsorption at the beginning to investigate the initial ammonia content of the sample (indicated by dotted lines in Figure 4). The main desorption peaks in the NH_3-TPD profiles of all samples are at 350–500 °C and the desorbed ammonia include the ammonia generated from the decomposition of the ammonium salts in the samples and the ammonia adsorbed at the acid sites of the samples. The contents of these two kinds of ammonia can be obtained according to the results of the above two temperature programmed desorption experiments. Generally, there may be both Lewis acid sites and Brønsted acid sites in acidic cesium salts of heteropolyacids. It has been considered that the ammonia desorption peak at lower temperature (<600 K) was due to the ammonia adsorbed at Lewis acid sites, while the desorption peak at higher temperature (>600 K) corresponded to the ammonia adsorbed on Brønsted acid sites [31]. Thus, the content of Brønsted acid sites of the compounds in this work can be estimated by the magnitude of the desorption peaks at 350–500 °C. Meanwhile, the content of protons in the compounds can be calculated because the Brønsted acid sites are associated with the protons. As listed in Table 2, the contents of NH_4^+ and H^+ in the compounds decrease obviously with increasing Cs^+ content. It should be noted that the theoretical sum value of Cs^+, NH_4^+ and H^+ per molecule of these HPCs is supposed to be 4 if the heteropolyanion is single $[PMo_{11}VO_{40}]^{4-}$, however, the calculated value is less than that for every sample. This inconformity might be attributed to the migration of V from heteropolyanions to counterions.

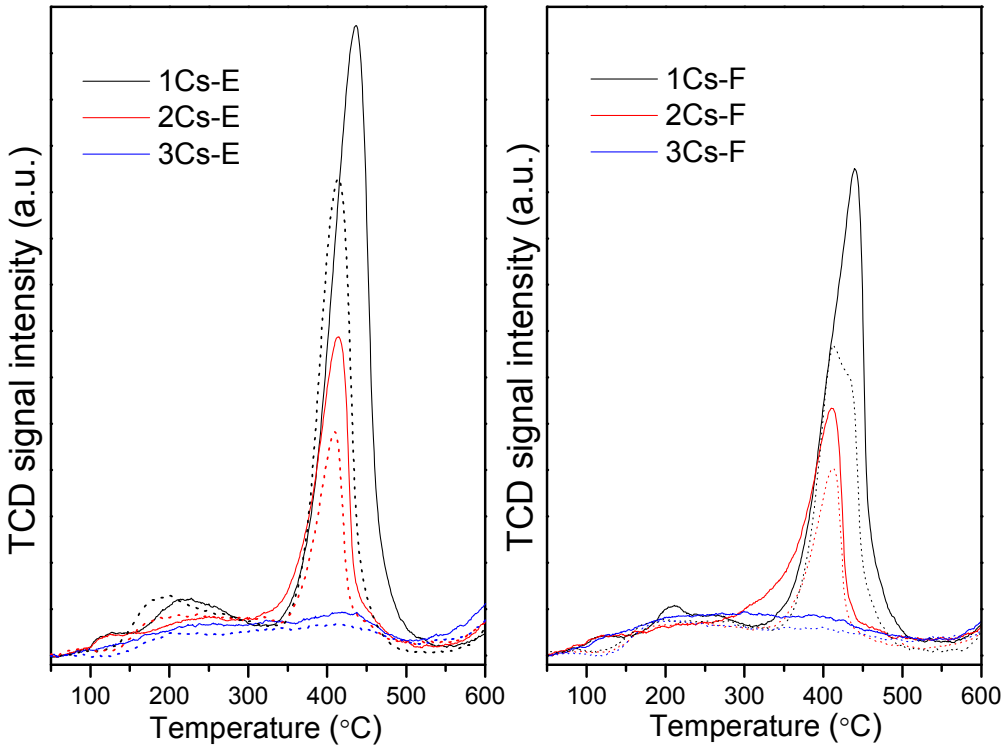

Figure 4. NH_3 temperature-programmed desorption (NH_3-TPD) profiles of the samples.

Table 2. The contents of NH_4^+ and H^+ in the compounds calculated from NH_3-TPD.

Sample	NH_4^+ (mmol·g^{-1})	H^+ (mmol·g^{-1})	Calculated Number of NH_4^+ and H^+ Per Molecule of the Mixed Heteropoly Salts	
			NH_4^+	H^+
1Cs-E	0.571	0.342	1.07	0.67
2Cs-E	0.214	0.161	0.44	0.33
3Cs-E	0.0235	0.0163	0.052	0.036
1Cs-F	0.444	0.237	0.90	0.48
2Cs-F	0.184	0.141	0.39	0.30
3Cs-F	0.0153	0.00075	0.033	0.002

2.5. Redox Property of the Calcined Compounds

The redox property of the calcined compounds was evaluated by H_2 temperature-programmed reduction (H_2-TPR) and the profiles are shown in Figure 5. There is a single reduction peak in the temperature range of 500–600 °C for every sample, which can be attributed to the reduction of Mo^{6+} to a lower valence state Mo^{5+} and/or Mo^{4+} [32]. Because the Keggin structure starts to decompose below 500 °C, the reduction peaks in the 500–600 °C range represent not only the reduction of octahedrally coordinated Mo^{6+} in the Keggin anions, but also the reduction of MoO_3 formed by the decomposition of the Keggin anions during the H_2-TPR experiments [33]. As can be seen in Figure 5, both preparation method and Cs^+ content have effects on the redox property of the compounds. The compounds prepared by using the evaporation residues as the precursors exhibit lower reduction temperature than the compounds prepared by using the initial precipitates as the precursors, and the reduction temperature decreased with the increase of Cs^+ content under the same preparation condition. Shoulder peaks are obviously found beside the main reduction peaks in the profiles of 2Cs-E and 2Cs-F. The maximum of the reduction peak is at 560 °C and the shoulder peak appears at 592 °C for 2Cs-E. Comparatively, the maximum of the reduction peak is at 592 °C and the shoulder peak appears at 568 °C for 2Cs-F. There are probably two types of Mo^{6+} species existing in these two samples and the difference of their relative amount might be due to the different preparation methods. Moreover, Cs^+ content is found to influence the relative amount of the Mo^{6+} species. Under the same preparation condition, the increase of Cs^+ content leads to the increase of the Mo^{6+} species with low reduction temperature and the decrease of the one with high reduction temperature.

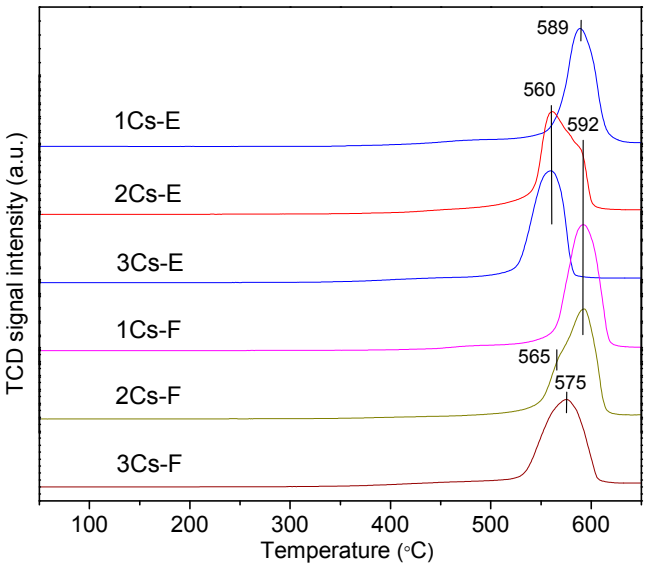

Figure 5. H_2 temperature-programmed reduction (H_2-TPR) profiles of the samples.

2.6. Textural Properties of the Calcined Compounds

The textural properties of the calcined compounds including the specific surface area, the porous volume and the average pore size were evaluated by N_2 adsorption-desorption experiment and the results are shown in Table 3. The increase of the surface areas with increasing Cs^+ content is observed for the samples prepared by two different ways, which is consistent with the results reported in the literature [18,19]. 3Cs-E and 3Cs-F are quite similar in chemical and phase compositions according to the characterizations of ICP-AES, FT-IR, XRD and NH_3-TPD, however there is a remarkable disparity in the surface areas between them. Besides, the average pore size of 3Cs-F is much smaller than that of 3Cs-E. As shown in Figure 6, the comparison of 3Cs-E and 3Cs-F in pore distribution reveals that there are more micropores in 3Cs-F than in 3Cs-E. The pore size distribution of 3Cs-F is mainly less than 7.7 nm and the largest amount of pores distributes at approximate 2 nm. Comparatively, in the pore size distribution of 3Cs-E, there is a relatively sharp peak with a maximum at 3.8 nm and a little one at 10.9 nm, as well as a rather broad one between 11.8 and 148.5 nm. The pore size distribution of 2Cs-F is quite similar to that of 3Cs-E except that the content of the pores with the diameter of 3.8 nm is much higher in 2Cs-F than in 3Cs-E. The pore volume of 2Cs-E is significantly higher than that of the other samples, and the pores in 2Cs-E distribute between 6.5 and 136.2 nm with a maximum at 22.5 nm, showing that 2Cs-E mainly contains large mesopores and macropores. There is no dominant peak in the pore size distribution of 1Cs-E and 1Cs-F. 1Cs-E shows low specific surface area (3.54 $m^2 \cdot g^{-1}$) and there might be only a small amount of aggregated pores with an average pore size of 42.8 nm, suggesting a nonporous structure in the bulk of it. The above results indicate that both preparation conditions and Cs^+ content have great effects on the textural properties of the compounds.

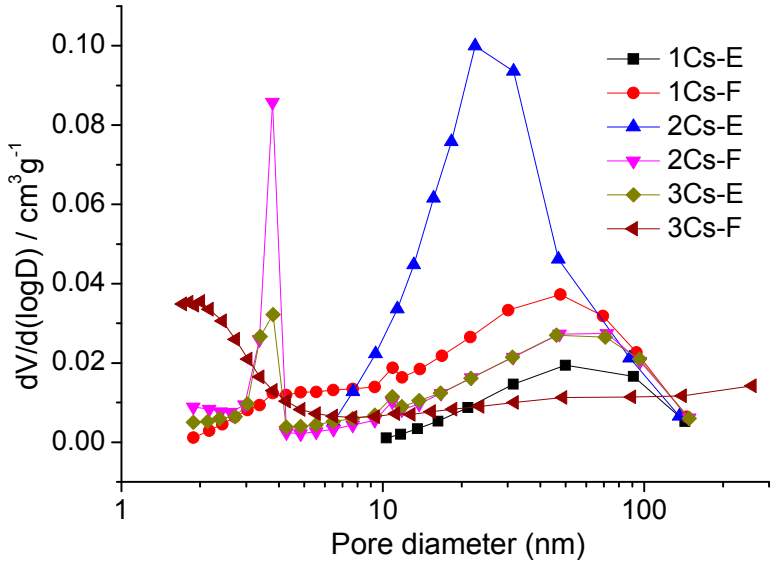

Figure 6. Pore size distribution of the samples.

Table 3. Textural properties of the samples.

Sample	S_{BET} ($m^2 \cdot g^{-1}$)	Pore Volume ($cm^3 \cdot g^{-1}$)	Average Pore Size (nm)
1Cs-E	3.54	0.016	42.8
1Cs-F	8.94	0.041	15.6
2Cs-E	13.9	0.067	23.6
2Cs-F	21.1	0.033	9.84
3Cs-E	14.6	0.031	12.4
3Cs-F	34.0	0.029	5.85

2.7. Catalytic Performance for the Oxidation of MAL to MAA

The mechanism for the selective oxidation of MAL to MAA has been proposed as a two-step reaction [34]. The first step reaction, which related to the formation of the intermediates having C–O–Mo bonds, is catalyzed by acid sites and the second step reaction refers to the oxidation of the intermediates to MAA catalyzed by the lattice oxygen of the HPCs. Thus, acidity and redox property, as well as the specific surface area and pore structure of the catalysts might have effects on the performance for this heterogeneous catalysis reaction. The performance of the catalysts for the oxidation of MAL to MAA after 6 h reaction at 300 °C is shown in Figure 7. It is found that the acidity and the specific surface area of the catalysts have significant effects on the catalytic performance. The selectivity of MAA on 1Cs-E has little difference comparing with that on 2Cs-E, but the conversion of MAL on 2Cs-E is much higher than that on 1Cs-E, which can be associated with the remarkable disparity in the specific surface area of them and a quite similar situation is found in the comparison between 1Cs-F and 2Cs-F. The comparison of 3Cs-E and 3Cs-F in catalytic performance revealed that the increase of specific surface area only improved the conversion of MAL, but not the selectivity of MAA. Though there are large differences in the pore size distribution among the catalysts, there is not a correlation between that and the catalytic performance, which suggests that the reaction is not controlled by diffusion. In our previous work [16], it was found that the existence of Cu and Fe as counterions in the acidic cesium salt of molybdovanadophosphoric acid can bring great enhancement of the redox property of the catalyst, resulting in the increase of the catalytic activity. As for the catalysts in this work, the reduction temperatures are relatively high and not different greatly from each other. Therefore, there are not obvious disparities in catalytic activity aroused by the redox property of the catalysts. In this condition, the acidities of the catalysts have the major effect on the selectivity of MAA. According to the results of NH_3-TPD measurement, significant decrease in solid acid sites and slight decline in acid strength were found with the increase of Cs adding amount in the catalysts. For the catalysts prepared by using the initial precipitates as the precursors, the selectivity reduces in the order of 1Cs-F, 2Cs-F and 3Cs-F. Especially, the selectivity on 3Cs-F dropped drastically compared to the other two catalysts. The decrease of acidity is considered to be the reason for the decrease of the selectivity. The catalysts prepared by using the evaporation residues as the precursors all exhibit lower catalytic performances than the catalysts prepared by using the initial precipitates as the precursors with the same Cs adding amount in the preparation process, even though they have comparatively higher acid amount. This should be due to the differences of the structure and textural properties caused by these two different preparation methods, as revealed by ^{31}P MAS NMR and N_2 adsorption-desorption measurements.

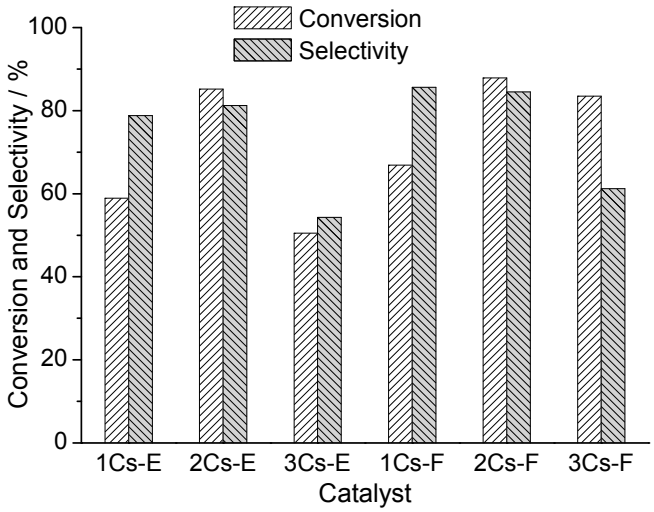

Figure 7. Catalytic performances of the catalysts.

3. Materials and Methods

3.1. Synthesis

MoO_3, NH_4VO_3, $CsNO_3$ and H_3PO_4 (85 wt %) were analytical grade and obtained from Sinopharm Chemical Reagent Beijing Co., Ltd., Beijing, China. The materials were used without any further treatment.

In a typical procedure, MoO_3 (7.9167 g), NH_4VO_3 (0.5849 g), 85 wt % H_3PO_4 (0.5765 g) and deionized water (75 mL) were added to a three-neck flask and heated to reflux under vigorously stirring for 7 h. $CsNO_3$ (0.9746 g) was dissolved in 50 mL of deionized water and dropped into the flask at 80 °C, and the molar ratio of $CsNO_3/MoO_3/NH_4VO_3/H_3PO_4$ was 1:11:1:1. After 3 h of reaction, the resulting suspension was evaporated to dryness at 80 °C to obtain the precursor of the catalyst with the nominal composition $Cs(NH_4)H_2PMo_{11}VO_{40}$, and then it was tableted with the addition 2 wt % by weight of graphite and calcined at 360 °C in air for 12 h. The obtained sample were crushed and sieved to the mesh size of 0.35–0.83 mm to be used as the catalyst and designated as 1Cs-E. In the above procedure, two catalysts were prepared and designated as 2Cs-E and 3Cs-E with the $CsNO_3$ adding amount as 1.9491 and 2.9237 g, i.e., the molar ratios of $CsNO_3/MoO_3/NH_4VO_3/H_3PO_4$ was 2:11:1:1 and 3:11:1:1, respectively. In the preparation process described above, the initial precipitates were separated out by filtration and washed to get the precursors, then they were tableted and calcined by the same procedure to get another series of catalysts, which were designated as 1Cs-F, 2Cs-F and 3Cs-F according to the different $CsNO_3$ adding amount, which were 0.9746, 1.9491 and 2.9237 g, respectively. The weighing error in the experiments was less than 0.1%.

3.2. Characterization

The elemental content of the samples were determined by ICP-AES on a Shimadzu ICPE-9000 apparatus (Shimadzu Corporation, Kyoto, Japan). FT-IR spectra were recorded on a Thermo Nicolet 6700 spectrophotometer (Thermo Fisher Scientific, Waltham, MA, USA) with anhydrous KBr as standard. XRD patterns were recorded on a Bruker D8-Advance X-ray powder diffractometer (Bruker AXS GmbH, Karlsruhe, Germany) operated at an accelerating voltage of 40 kV and an emission current of 40 mA with Cu Kα radiation. Solid-state MAS NMR experiments were carried out at room temperature on a Bruker Avance III 500 spectrometer (Bruker BioSpin AG, Zurich, Switzerland) with a spinning frequency of 7 kHz, The chemical shift (δ) of spectra was referenced to 85% H_3PO_4 (δ = 0 ppm). NH_3-TPD and H_2-TPR measurements were carried out on a Micromeritics Autochem II 2920 apparatus (Micromeritics Instrument Corporation, Norcross, GA, USA). In a typical NH_3-TPD experiment, 40 mg of sample was pretreated in a helium flow at 150 °C with a heating rate of 10 °C·min^{-1} and the sample was kept at this temperature for 1 h. Subsequently the sample was treated with a 10% NH_3-He flow for 30 min at room temperature, then the sample was purging in a helium flow for 1 h at 100 °C, until the baseline was stable, the desorption profile was measured by the thermal conductivity detector in flowing helium at a heating rate of 10 °C·min^{-1} to 600 °C. In a typical H_2-TPR experiment, 90 mg of sample was pretreated in a helium flow at 150 °C with a heating rate of 10 °C·min^{-1} and the sample was kept at this temperature for 1 h. After pretreatment, the sample was cooled to 50 °C. Until the baseline was stable, the TPR analysis was carried out in a 10% H_2-Ar flow at a heating rate of 10 °C·min^{-1} to 650 °C. Nitrogen adsorption-desorption isotherms were measured using a Micromeritics ASAP 2460 surface area and porosity analyzer (Micromeritics Instrument Corporation) and the specific surface areas were calculated using the Brunauer–Emmett–Teller (BET) equation. The mean pore diameters were calculated by the Barrett–Joyner–Halenda (BJH) method using the desorption curves.

3.3. Catalytic Activity Measurement

The selective oxidation of MAL to MAA was carried out in a fixed-bed reactor at atmospheric pressure. In a typical experiment, 1 mL catalyst was loaded into the constant temperature zone of

a stainless steel tubular reactor and quartz sand was used to fill up the leaving space of the reactor. MAL was delivered with a steady flow rate 2.7×10^{-3} mol·h^{-1} by a N_2 flow to a mixer kept at 150 °C. Air and steam were also continuously fed into the mixer. After mixing the gaseous reactants were directed into the reactor with a mole ratio of $MAL/O_2/N_2/H_2O$ = 1:2.5:15:8 and the reaction temperature was maintained at 300 °C. After the catalytic reaction was carried out for 6 h, the products were gathered and analyzed by an Agilent 6890 gas chromatograph (Agilent Technologies, Santa Clara, CA, USA) equipped with a flame ionization detector (FID) detector using a DB-624 capillary column.

4. Conclusions

The elemental analysis can be used to speculate the phase composition of the precipitates in the slurry. The increase in Cs^+ adding amount promotes the substitution of V for Mo in the heteropolyanions during the preparation process of the precursors and enhances the stability of the $[PMo_{11}VO_{40}]^{4-}$ heteropolyanions during calcination. Both the initial precipitates and the evaporation residues are mixtures of cesium and ammonium salts of heteropolyacids before calcination. Thermal treatment causes the decomposition of the ammonium salts and the formation of single-phase solid solution from a mechanical mixture. Both NH_4^+ and H^+ in the calcined compounds decrease obviously with the increase in Cs^+ content. The catalysts prepared using the evaporation residues as the precursors exhibit lower reduction temperature than the catalysts prepared using the initial precipitates as the precursors, and the reduction temperature decreased with the increase of Cs^+ content under the same preparation condition. Both preparation conditions and Cs^+ content have great effects on the textural properties of the catalysts. For this series of catalysts, the determinants of the catalytic performance are acidity and specific surface area, and the former mainly affects the selectivity of MAA, while the latter mainly affects the conversion of MAL.

Acknowledgments: This work is financially supported by the National Natural Science Foundation of China (21206179), the Natural Science Foundation of Shandong Province (ZR2012BQ015), and the State Key Laboratory of Chemical Engineering, China (SKL-ChE-15A03).

Author Contributions: Heng Zhang conceived and designed the experiments; Heng Zhang, Tingting Wang and Xinxin Ma performed the experiments; Heng Zhang analyzed the data and wrote the paper; Wancheng Zhu contributed to the analysis of the data.

Conflicts of Interest: The authors declare no conflict of interest.

References

1. Tungatarova, S.A.; Abdukhalykov, D.B.; Baizhumanova, T.S.; Komashko, L.V.; Grigorieva, V.P.; Chanysheva, I.S. Oxidation of alkanes into olefins on the polyoxide catalysts. *Catal. Today* **2015**, *256*, 276–286. [CrossRef]
2. Kuznetsova, N.I.; Popova, G.Y.; Kuznetsova, L.I.; Zaikovskii, V.I.; Koscheev, S.V.; Andrushkeich, T.V.; Lisitsyn, A.S.; Likholobov, V.A.; Han, S. Improving the performance of Pt-$H_3PMo_{12}O_{40}$ catalysts in the selective dehydrogenation of propane with O_2 and H_2. *Catal. Today* **2015**, *245*, 179–185. [CrossRef]
3. Mizuno, N.; Tateishi, M.; Iwamoto, M. Pronounced catalytic activity of $Fe_{0.08}Cs_{2.5}H_{1.26}PVMo_{11}O_{40}$ for direct oxidation of propane into acrylic acid. *Appl. Catal. A* **1995**, *128*, L165–L170. [CrossRef]
4. Liu, L.; Ye, X.P.; Bozell, J.J. A comparative review of petroleum-based and bio-based acrolein production. *ChemSusChem* **2012**, *5*, 1162–1180. [CrossRef] [PubMed]
5. Liu, S.; Chen, L.; Wang, G.; Liu, J.; Gao, Y.; Li, C.; Shan, H. Effects of Cs-substitution and partial reduction on catalytic performance of Keggin-type phosphomolybdic polyoxometalates for selective oxidation of isobutene. *J. Energy Chem.* **2016**, *25*, 85–92. [CrossRef]
6. Nagai, K. New developments in the production of methyl methacrylate. *Appl. Catal. A* **2001**, *221*, 367–377. [CrossRef]
7. Li, X.K.; Zhang, Y.G. Oxidative dehydration of glycerol to acrylic acid over vanadium-substituted cesium salts of Keggin-type heteropolyacids. *ACS Catal.* **2016**, *6*, 2785–2791. [CrossRef]

8. Srinivas, M.; Raveendra, G.; Parameswaram, G.; Sai Prasad, P.S.; Lingaiah, N. Cesium exchanged tungstophosphoric acid supported on tin oxide: An efficient solid acid catalyst for etherification of glycerol with *tert*-butanol to synthesize biofuel additives. *J. Mol. Catal. A* **2016**, *413*, 7–14. [CrossRef]
9. Costa, V.V.; da Silva Rocha, K.A.; Oliveira, L.C.A.; Kozhevnikova, E.F.; Kozhevnikov, I.V.; Gusevskaya, E.V. Heteropoly acid catalysts for the synthesis of fragrance compounds from bio-renewables: Acetylation of nopol and terpenic alcohols. *RSC Adv.* **2016**, *6*, 43217–43222. [CrossRef]
10. Trautwein, G.; El Bakkali, B.; Alcaniz-Monge, J.; Artetxe, B.; Reinoso, S.; Gutierrez-Zorrilla, J.M. Dimeric assemblies of lanthanide-stabilised dilacunary Keggin tungstogermanates: A new class of catalysts for the selective oxidation of aniline. *J. Catal.* **2015**, *331*, 110–117. [CrossRef]
11. Mizuno, N.; Misono, M. Heterogeneous catalysis. *Chem. Rev.* **1998**, *98*, 199–217. [CrossRef] [PubMed]
12. Stytsenko, V.D.; Lee, W.H.; Lee, J.W. Catalyst design for methacrolein oxidation to methacrylic acid. *Kinet. Catal.* **2001**, *42*, 212–216. [CrossRef]
13. Bayer, R.; Marchal, C.; Liu, F.X.; Tézé, A.; Hervé, G. Catalysis of the oxidation of isobutyric acid by vanadyl, copper and mixed vanadyl-copper salts of $H_3[PMo_{12}O_{40}]$ and $H_4[PMo_{11}VO_{40}]$. *J. Mol. Catal. A* **1996**, *114*, 277–286. [CrossRef]
14. Zhou, L.L.; Wang, L.; Zhang, S.J.; Yan, R.Y.; Diao, Y.Y. Effect of vanadyl species in Keggin-type heteropoly catalysts in selective oxidation of methacrolein to methacrylic acid. *J. Catal.* **2015**, *329*, 431–440. [CrossRef]
15. Kendell, S.M.; Alston, A.S.; Ballam, N.J.; Brown, T.C.; Burns, R.C. Structural and activity investigation into Al^{3+}, La^{3+} and Ce^{3+} addition to the phosphomolybdate heteropolyanion for isobutane selective oxidation. *Catal. Lett.* **2011**, *141*, 374–390. [CrossRef]
16. Zhang, H.; Yan, R.Y.; Yang, L.; Diao, Y.Y.; Wang, L.; Zhang, S.J. Investigation of Cu- and Fe-doped $CsH_3PMo_{11}VO_{40}$ heteropoly compounds for the selective oxidation of methacrolein to methacrylic acid. *Ind. Eng. Chem. Res.* **2013**, *52*, 4484–4490. [CrossRef]
17. Zheng, Y.X.; Zhang, H.; Wang, L.; Zhang, S.J.; Wang, S.J. Transition metal-doped heteropoly catalysts for the selective oxidation of methacrolein to methacrylic acid. *Front. Chem. Sci. Eng.* **2016**, *10*, 139–146. [CrossRef]
18. Lee, K.Y.; Oishi, S.; Igarashi, H.; Misono, M. Acidic cesium salts of molybdovanadophosphoric acids as efficient catalysts for oxidative dehydrogenation of isobutyric acid. *Catal. Today* **1997**, *33*, 183–189. [CrossRef]
19. Jing, F.; Katryniok, B.; Dumeignil, F.; Bordes-Richard, E.; Paul, S. Catalytic selective oxidation of isobutane over $Cs_x(NH_4)_{3-x}HPMo_{11}VO_{40}$ mixed salts. *Catal. Sci. Technol.* **2014**, *4*, 2938–2945. [CrossRef]
20. Santos, J.S.; Dias, J.A.; Dias, S.C.L.; Garcia, F.A.C.; Macedo, J.L.; Sousa, F.S.G.; Almeida, L.S. Mixed salts of cesium and ammonium derivatives of 12-tungstophosphoric acid: Synthesis and structural characterization. *Appl. Catal. A* **2011**, *394*, 138–148. [CrossRef]
21. Langpape, M.; Millet, J.M.M.; Ozkan, U.S.; Boudeulle, M. Study of cesium or cesium-transition metal-substituted Keggin-type phosphomolybdic acid as isobutane oxidation catalysts: I. Structural characterization. *J. Catal.* **1999**, *181*, 80–90. [CrossRef]
22. Villabrille, P.; Romanelli, G.; Vázquez, P.; Cáceres, C. Vanadium-substituted Keggin heteropolycompounds as catalysts for ecofriendly liquid phase oxidation of 2,6-dimethylphenol to 2,6-dimethyl-1, 4-benzoquinone. *Appl. Catal. A* **2004**, *270*, 101–111. [CrossRef]
23. Mizuno, N.; Suh, D.; Han, W.; Kudo, T. Catalytic performance of $Cs_{2.5}Fe_{0.08}H_{1.26}PVMo_{11}O_{40}$ for direct oxidation of lower alkanes. *J. Mol. Catal. A* **1996**, *114*, 309–317. [CrossRef]
24. Ilkenhans, T.; Herzog, B.; Braun, T.; Schlögl, R. The nature of the active phase in the heteropolyacid catalyst $H_4PVMo_{11}O_{40}{\cdot}32H_2O$ used for the selective oxidation of isobutyric acid. *J. Catal.* **1995**, *153*, 275–292. [CrossRef]
25. Marosi, L.; Platero, E.E.; Cifre, J.; Areán, C.O. Thermal dehydration of $H_{3+x}PV_xM_{12-x}O_{40}{\cdot}yH_2O$ Keggin type heteropolyacids; formation, thermal stability and structure of the anhydrous acids $H_3PM_{12}O_{40}$, of the corresponding anhydrides $PM_{12}O_{38.5}$ and of a novel trihydrate $H_3PW_{12}O_{40}{\cdot}3H_2O$. *J. Mater. Chem.* **2000**, *10*, 1949–1955. [CrossRef]
26. Dimitratos, N.; Védrine, J.C. Study of Ga modified $Cs_{2.5}H_{1.5}PV_1Mo_{11}O_{40}$ heteropolyoxometallates for propane selective oxidation. *J. Mol. Catal. A* **2006**, *255*, 184–192. [CrossRef]
27. Okuhara, T.; Noritaka, N.; Misono, M. Catalytic chemistry of heteropoly compounds. *Adv. Catal.* **1996**, *41*, 113–252.

28. Dimitratos, N.; Védrine, J.C. Properties of $Cs_{2.5}$ salts of transition metal M substituted Keggin-type $M_{1-x}PV_1M_xMo_{11-x}O_{40}$ heteropolyoxometallates in propane oxidation. *Appl. Catal. A* **2003**, *256*, 251–263. [CrossRef]
29. Spojakina, A.A.; Kostova, N.G.; Sow, B.; Stamenova, M.W.; Jiratova, K. Thiophene conversion and ethanol oxidation on SiO_2-supported 12-PMoV-mixed heteropoly compounds. *Catal. Today* **2001**, *65*, 315–321. [CrossRef]
30. Molinari, J.E.; Nakka, L.; Kim, T.; Wachs, I.E. Dynamic surface structures and reactivity of vanadium-containing molybdophosphoric acid ($H_{3+x}PMo_{12-x}V_xO_{40}$) Keggin catalysts during methanol oxidation and dehydration. *ACS Catal.* **2011**, *1*, 1536–1548. [CrossRef]
31. Sun, M.; Zhang, J.; Cao, C.; Zhang, Q.; Wang, Y.; Wan, H. Significant effect of acidity on catalytic behaviors of Cs-substituted polyoxometalates for oxidative dehydrogenation of propane. *Appl. Catal. A* **2008**, *349*, 212–221. [CrossRef]
32. Damyanova, S.; Spojakina, A.; Jiratova, K. Effect of mixed titania-alumina supports on the phase composition of $NiMo/TiO_2$–Al_2O_3 catalysts. *Appl. Catal. A* **2007**, *125*, 257–269. [CrossRef]
33. Damyanova, S.; Cubeiro, M.L.; Fierro, J.L.G. Acid-redox properties of titania-supported 12-molybdophosphates for methanol oxidation. *J. Mol. Catal. A* **1999**, *142*, 85–100. [CrossRef]
34. Misono, M.; Nojiri, N. Recent progress in catalytic technology in Japan. *Appl. Catal.* **1990**, *64*, 1–30. [CrossRef]